

1 **Investigations on the Effect of Current Density on SiO/Si Composite**

2 **Electrodes**

3 Jie Xiong<sup>a</sup>, Jian Yang<sup>a</sup>, Guanyi Wang<sup>a</sup>, Tahseen Saeed<sup>a</sup>, Yuze Liu<sup>b</sup>, Stephen E  
4 Kaczmarek<sup>c</sup>, Wenquan Lu<sup>d,\*</sup>, Qingliu Wu<sup>a,\*</sup>

5 a- Department of Chemical and Paper Engineering, Western Michigan University,  
6 4601 Campus Drive, Kalamazoo, Michigan, 49008-5462, U. S.A.

7 b- Center for Nanoscale Materials, Argonne National Laboratory, 9700 South Cass  
8 Ave., Lemont, Illinois, 60439-4837, U. S. A.

9 c- Department of Geological and Environmental Sciences, Western Michigan  
10 University, 1903 W. Michigan Ave., Kalamazoo, Michigan, 49008-5241, U. S. A.

11 d- Chemical Science and Engineering Division, Argonne National Laboratory, 9700  
12 South Cass Ave., Lemont, Illinois, 60439-4837, U. S. A.

13  
14 \* Correspondence should be addressed to:

15 Wenquan Lu; email: [wenquan.lu@anl.gov](mailto:wenquan.lu@anl.gov); Phone: 630-252-3704, Fax: 630-252-4176

16 Qingliu Wu, email: [qingliu.wu@wmich.edu](mailto:qingliu.wu@wmich.edu); Phone: 269-276-3998; Fax: 269-276-3501

1 **Abstract:**

2 An oxide layer on the surface of silicon particles is inevitable and is necessary for their  
3 application as anode materials for lithium ion batteries with high capacity and durability.  
4 However, a thick surficial oxide layer could significantly reduce the capacity of a Si anode.  
5 In this study, Si nanoparticles with a thick surficial oxide layer of ~20 nm (Si@SiO<sub>x</sub>) were  
6 fabricated through thermal oxidation and investigated electrochemically. The results  
7 revealed that very low current density is needed to activate Si@SiO<sub>x</sub> anodes during the first  
8 formation cycle. Once activated, the Si@SiO<sub>x</sub> anode can deliver reversible capacity as high  
9 as ~1000 mAh/g with low current density. Then, the Si@SiO<sub>x</sub> can be cycled at higher  
10 current densities of >700 mAh/g. Electrochemical impedance spectroscopy (EIS) shows  
11 that the lower current density results in lower charge-transfer resistance of the Si@SiO<sub>x</sub>  
12 anode, suggesting a higher degree of lithiation of the surficial oxide layer during low-  
13 current activation. EIS analysis also reveals that the lithiation of the surficial oxide is  
14 irreversible. We believe that the surface silicon oxide layer is lithiated and forms lithium  
15 silicate during the initial activation process. Lithium silicate has high conductivity and  
16 allows the lithiation/delithiation of Si core under the oxide layer during following charge  
17 and discharge.

18 **Key words:** Silicon anode, silicon oxide layer, current density, lithium batteries

19

## 1 **1. Introduction**

2 Silicon has been considered as one of the most promising anode candidates for  
3 lithium-ion batteries (LIBs) because of its extremely high theoretical capacity of 4200  
4 mAh/g, which is 10 times higher than that of graphite anodes.[1, 2] However, the wide  
5 adoption of Si anodes in commercial LIBs is hindered by their notoriously fast capacity  
6 decay, originating from their poor conductivity[3] and large volume change during the  
7 lithium insertion/extraction process[4]. The large volume change results in the repeated  
8 generation of cracks, leading to the continuous growth of a solid-electrolyte interface (SEI)  
9 film at the surface of the Si,[5] degradation of the electronic connectivity of the electrode,  
10 and consequently the capacity decay of the cell. Further, the propagation of cracks will  
11 cause the Si to pulverize and peel off from the electrode,[6] accelerating the capacity fading  
12 of the LIB. To address these issues, various strategies have been developed.

13 Fabricating nano-featured Si with the objective of suppressing the formation and  
14 propagation of cracks is an effective approach to improving the cycle life of Si anodes.  
15 Successful examples include Si nanowire,[7] Si nanoparticles,[8] Si thin films,[9] and Si  
16 nanotubes.[10] These approaches can effectively mitigate the Si pulverization and peeling  
17 off of active material from the current collector, but have little effect on suppressing the  
18 formation of SEI films. This shortcoming has led to efforts to develop Si anodes with inert  
19 coatings, including Si-based composites such as Si/C composite,[11] Si/graphene,[12] and  
20 Si-based alloys,[13] to suppress the formation and growth of the SEI films. These coating  
21 materials are generally carbonaceous materials, such as amorphous carbon,[14]  
22 graphene,[12] and carbon nanotubes.[15] Recently, silicon oxide, a native oxide layer  
23 formed at the surface of Si products when they are exposed to the air, has emerged as a

1 promising coating material to improve the performance of Si anodes. Owing to the stronger  
2 bond energy of Si-O relative to Si-Si,[16] this surficial oxide layer has two functions in Si-  
3 based anodes: One is to act as a barrier preventing direct contact between the Si and the  
4 electrolyte, and the other is to provide a mechanically constrained interface during both  
5 lithiation and delithiation. Thus, this bifunctional surficial oxide layer could enable the  
6 formation of a stable SEI at the surface of active materials and significantly improve the  
7 electrochemical performance of Si-based anodes. The presence of this surficial oxide layer  
8 could effectively improve the durability of Si-based anodes, such as double-walled Si-SiO<sub>x</sub>  
9 nanotube (DWSiNT) anodes,[17] SiO<sub>x</sub>-coated Si nanowire anodes,[18] and nanosized Si  
10 anodes coated with SiO<sub>x</sub>. [19] However, the improved durability of oxide-coated Si anodes  
11 is a trade-off for reduced specific capacity.[20] Furthermore, increasing the thickness of  
12 the surficial oxide layer could significantly reduce the capacity of Si anodes,[19] and it  
13 even leads to a negligible capacity when the thickness of the surficial oxide layer is >6  
14 nm.[21] Given the promise for improving the durability of LIBs, it is still very worthwhile  
15 to develop an effective approach to extract a high capacity from Si anodes with thick  
16 surficial oxide coating. Apparently, an in-depth understanding of the lithiation mechanism  
17 of oxide-coated Si is crucial.

18 To date, the lithiation mechanism of oxide-coated Si is still ambiguous. Using  
19 finite-element simulations, McDowell and co-workers proposed that the formation of a  
20 surficial oxide layer can induce a compressive hydrostatic stress in a Si anode.[16] This  
21 oxide-induced stress could suppress the volume expansion and consequently limit the  
22 extent of lithiation in the Si anode. This study successfully revealed the thermodynamic  
23 effect of the surficial oxide layer on the behavior of the Si core, but was unable to elucidate

1 the lithiation process occurring in oxide-coated Si, especially the lithiation of the surficial  
2 oxide layer. There is no doubt that the Si lithiation is reversible, but the lithiation of silica  
3 is still a matter of controversy. A few studies have reported that SiO<sub>2</sub> lithiation is largely  
4 irreversible because of the formation of the irreversibly lithiated products Li<sub>4</sub>SiO<sub>4</sub> and  
5 Li<sub>2</sub>O.[22, 23] However, the reversible lithiation of SiO<sub>2</sub>[24, 25] and the at least partially  
6 reversible formation of Li<sub>4</sub>SiO<sub>4</sub>[26] have been reported by other researchers. It has also  
7 been reported that, when the surficial SiO<sub>2</sub> coating on a Si wafer anode is thicker than 3  
8 nm, a localized lithiation along the pinholes existing in the surficial oxide layer dominates,  
9 leading to the initiation of lithiation at negative voltages or at long-duration positive  
10 voltages.[27] However, the occurrence of lithiation above 0.01 V (vs. Li<sup>+</sup>/Li) at a rate of  
11 0.2 C has also been observed on Si nanowires with 7-nm or thicker SiO<sub>2</sub> coatings.[20]  
12 Furthermore, the type of lithium salt in the electrolyte can profoundly influence the  
13 lithiated products in the surficial oxide layer and consequently the lithiation process of  
14 silica at the surface of a Si anode.[28] Regardless of these divergent observations and  
15 mechanisms of silicate lithiation, it is well known that lithiated silicate products, such as  
16 Li<sub>4</sub>SiO<sub>4</sub> and Li<sub>2</sub>O, are superior to the original SiO<sub>2</sub> in both electronic and ionic  
17 conductivity.[29, 30] In addition, it has been reported that the lithiation of silica is a kinetic  
18 process and strongly depends on the operating conditions. In particular, the formation of  
19 lithiated silicate is favored at low current density.[31] This observation inspired us to  
20 initiate the lithiation of a thick surficial oxide at low current density and take advantage of  
21 the conductive lithiated silica coating to exploit the high capacity of the Si core, with high  
22 current density in the following cycles.

1           In the present study, Si particles with an ~20-nm-thick surficial oxide layer were  
2 prepared by thermally oxidizing Si nanoparticles at ambient atmosphere, and the as-  
3 synthesized Si@SiO<sub>x</sub> composite was utilized as the LIB anode. The effect of current  
4 density during the initial cycle on the utilization of active Si was studied. Meanwhile, the  
5 root cause of low utilization of active Si with a thick surficial oxide layer was also  
6 investigated.

## 7 **2. Experimental**

### 8 **2.1. Material preparation**

9           To prepare Si@SiO<sub>x</sub> powders, Si nanoparticles (average size of ~80 nm) contained  
10 in an alumina crucible were placed inside a muffle furnace. The temperature of the furnace  
11 was increased from room temperature to various temperatures with a ramp of 25°C/min  
12 and kept at the targeted temperatures for 15 h. After they cooled down to room temperature  
13 naturally, the resulting Si@SiO<sub>x</sub> powders were kept in a desiccator for further  
14 characterization and applications. The mass weights of the Si samples before and after  
15 thermal treatment were recorded. On the basis of the weight gain, the thickness of the  
16 surficial oxide layer in the Si@SiO<sub>x</sub> samples obtained at various temperatures was  
17 calculated by using the method of Zhang et al.[21] Details of the calculation can be found  
18 in the Supporting Information.

### 19 **2.2. Material characterizations**

20           Phase information for pristine and thermally treated Si nanoparticles was  
21 determined by using X-ray diffraction (XRD) analysis, performed on a Bruker D2 Phaser  
22 Diffractometer with a Cu K $\alpha$  ( $\lambda=1.5406\text{\AA}$ ). Scanning electron microscope (SEM) images

1 were collected with a JEOL IT-100 InTouch microscope at 3 kV. To accurately measure  
2 the thickness of the surficial oxide layer, the thermally treated Si was examined with a  
3 JEM-2010F high-resolution transmission electron microscope (TEM) at an accelerating  
4 voltage of 200 kV. The Fourier-transform infrared spectroscopy (FTIR) measurements  
5 were performed on a PerkinElmer 100 FTIR spectrophotometer to identify compounds of  
6 thermally treated Si powders, as-prepared Si anode and cycled Si anodes. FTIR spectra  
7 were collected in an attenuated total reflectance (ATR) mode at 600-2000  $\text{cm}^{-1}$  with a  
8 resolution of 4  $\text{cm}^{-1}$ . Before FTIR analysis, the cycled electrodes were harvested from cells  
9 underwent discharge with the current density of 10 mA/g following by charged to 1.5V,  
10 rinsed with dimethyl carbonate (DMC), and dried inside a glovebox.

### 11 **2.3. Electrode fabrication and cell assembly**

12 First, the active Si@SiO<sub>x</sub> material and carbon black were combined in an aqueous  
13 solution containing 10 wt.% polyacrylic acid (PAA), with continuous stirring. The  
14 resulting slurry was cast onto Cu foil, dried at 50°C for 2 hours, and then dried overnight  
15 at 120°C in a vacuum oven to completely remove the moisture. The final dried electrodes  
16 are composed of 70% active material, 10% carbon black, and 20% PAA binder. These  
17 electrodes were cut into 9/16-in.-diameter disks and assembled in 2032-type coin cells with  
18 lithium metal counter-electrodes. An electrolyte solution containing 10% fluoroethylene  
19 carbonate (FEC) and 1.2 mol/L LiPF<sub>6</sub> in ethylene carbonate/ethyl methyl carbonate (3/7  
20 by weight) was used in all cells.

### 21 **2.4. Electrochemical evaluations**

1 Galvanostatic cycling tests of Li/Si@SiO<sub>x</sub> half-cells were conducted on a Neware  
2 BTS-4000 cell tester; constant currents were applied at room temperature in the initial  
3 cycles. The voltage window applied to all cells was 0.001–1.5 V (vs. Li/Li<sup>+</sup>). The  
4 electrochemical data were used to calculate the thickness of the oxide layer at the surface  
5 of Si@SiO<sub>x</sub>; details about the calculation can be found in the Supporting Information.  
6 Electrochemical impedance spectroscopy (EIS) data were collected using a Gamry  
7 Interface 1010 Electrochemical Workstation system with a potential amplitude of 5 mV  
8 over the frequency range of 50 mHz–100 kHz. Before EIS measurement, cells were  
9 discharged or charged to various states and then rested for at least 4 hours.

### 10 **3. Results and Discussion**

11 The formation of an oxide layer at the surface of Si particles was first revealed by  
12 measuring the weight change of samples before and after the thermal treatment. **Figure 1**  
13 shows that the weight change of samples gradually increases as the temperature of thermal  
14 treatment increases to just below 800°C. Given the experimental conditions used here,  
15 involving only the oxidation reaction of Si in air, the weight gain implies the formation of  
16 an oxide layer on the surface of the Si particles, and the higher the sintering temperature,  
17 the thicker the oxide layer. However, the weight change of the samples remained constant  
18 when the sintering temperature was above 800°C. From the weight gain, the thickness of  
19 the surficial oxide layer could be calculated by using the method proposed by Zhang et  
20 al.[21] Calculated results show that the thickness of the oxide layer increases with the  
21 treatment temperature and reaches a constant value of ~19.6 nm when the treatment  
22 temperature is above 800°C (**Table 1**). This finding indicates that there is a limit to  
23 increasing the thickness of the oxide layer on the surface of Si powder through increasing

1 the temperature of the thermal process. Therefore, the following characterizations were  
2 carried out on samples that were either pristine or thermally treated at 800°C.

3 The formation of an oxide layer was further confirmed through XRD measurements  
4 (**Fig. 2**). Before the thermal treatment, all reflections could be identified as crystal Si  
5 ( $Fd\bar{3}m$ ,  $a = 5.42 \text{ \AA}$ ) without discernible secondary phase and/or impurities. The sharp  
6 diffraction peaks observed in the XRD pattern indicate that the pristine Si powders are  
7 highly crystalline. After thermal treatment at 800°C, a broad peak located at about 22° is  
8 found in addition to the sharp peaks belonging to Si crystal. This broad peak is ascribed to  
9 amorphous silica.[32] The effect of thermal treatment on the morphology of Si powder was  
10 revealed by SEM observations, as shown in **Fig. 3**. Before the thermal treatment, the  
11 pristine sample is composed of uniform particles with a spherical shape and an average  
12 size of ~80 nm (**Fig.3a**). After thermal treatment at 800°C, the spherical shape is still  
13 observable, but the particle outlines are severely blurred (**Fig. 3b**), indicative of the  
14 formation of an oxide layer with poor conductivity at the surface of the Si particles. The  
15 formation of a surficial oxide layer and its thickness could be further verified through TEM  
16 observations. A TEM image obtained from a representative Si particle after 800°C  
17 treatment clearly shows a boundary line between the inner core and outer shell (**Fig.3c**).  
18 The high-resolution TEM (HRTEM) image (**Fig. 3d**) shows that, across the whole field of  
19 view, a single orientation of lattice planes is observable on the inner core and the  
20 interplanary spacing is approximated to 3.3Å, corresponding to Si (111) lattice spacing of  
21 3.2Å. No lattice fringes are visible surrounding this Si crystal core, indicative of the  
22 coexistence of a crystalline core and an amorphous oxide shell in an individual Si particle.  
23 In further, the thickness of the oxide shell is measured to be ~21.7 nm (**Fig. 3e**). Given the

1 error in measurement, this agrees well with the calculated values based on the weight gain  
2 and electrochemical characterization, which will be discussed below.

3         The thermally treated Si powders (Si@SiO<sub>x</sub>) were used as the active materials of  
4 LIB anodes for electrochemical characterizations. **Figure 4** shows the voltage profiles of  
5 the Si@SiO<sub>x</sub> anodes during the initial formation cycle at various current densities. At a  
6 current density of 100 mA/g, only a slope-like feature with two shoulders, one located at  
7 ~1.5 V and the other at ~0.7 V, was found on the discharge (lithiation) curve (**Fig. 4b**), and  
8 an extremely low capacity of 68 mAh/g was delivered by the cell (**Fig. 4a**). The positions  
9 of the two shoulders moved to higher voltages when the current density was decreased (**Fig.**  
10 **4b**). In addition, a very short plateau at ~0.05 V was observable on the discharge curve  
11 when the current density was reduced to 20 mA/g (**Fig. 4b**). The specific capacity increased  
12 slightly when the current density was reduced, and reached ~71 mAh/g at 50 mA/g and ~  
13 97 mAh/g at 20 mA/g (**Fig. 4b**). Our observations here are consistent with reports from  
14 other researchers that an almost negligible capacity could be delivered by Si powders after  
15 thermal treatment at a temperature above 700°C.[21] It is believed that the existence of a  
16 surficial oxide could reduce the equilibrium concentration of Li in the Li-Si phase,[16]  
17 leading to a Si anode with very low capacity.[16, 20, 21, 33] However, an extremely long  
18 plateau at ~ 0.05 V was found on the discharge curve when the current density was further  
19 reduced to 10 mA/g (**Fig. 4a**). During the following charge (delithiation) process, a plateau-  
20 like feature was also found at ~0.4 V, characteristic of the transformation of crystallized  
21 Li-Si alloy to amorphous Si.[34] Correspondingly, an unprecedentedly high discharge  
22 capacity of ~1832 mAh/g was delivered by the cell at this low current density. Obviously,  
23 the current density plays a crucial role in the electrochemical performance of a Si anode

1 with a thick surficial oxide layer. It seems that there is a threshold value for the current  
2 density applied to the cell, below which the lithiation of Si wrapped by a thick oxide layer  
3 could take place. To the best of our knowledge, this is the **first** time a reported capacity  
4 of >1000 mAh/g was delivered by Si with such a thick surficial oxide layer. The Coulombic  
5 efficiency (CE) was calculated to be ~38% at a current density of 100 mA/g, and stayed  
6 constant even when the current density was reduced to 20 mA/g. However, the value of CE  
7 increased to 58% when the current density was reduced to 10 mA/g. The specific capacities  
8 and CEs measured for cells at various current densities are summarized in **Table 2**. Because  
9 the Si samples used here consist solely of nanoparticles, a large amount of solid electrolyte  
10 interface (SEI) film will inevitably form at the surface of the active materials. We believe  
11 that the formation of SEI film, combined with the irreversible reaction between silicon  
12 oxides and lithium, led to the low CE during the first cycle.

13         It is easier to see the effect of current density on the intercalation/deintercalation of  
14 lithium ions in the Si@SiO<sub>x</sub> anode through the analysis of differential capacity curves  
15 (dQ/dV vs. V) of cells in the first cycle, shown in **Fig. 5**. At the high current density of 100  
16 mA/g, two broad peaks are observed at ~1.5 V and ~0.7 V during the discharge process  
17 (**Fig. 5b**). Both broad peaks shift to higher voltages with decreasing current density, and  
18 reach ~1.7 V and ~1.0 V, respectively, at 10 mA/g. Given the potential range of ~0.4–1.0  
19 V for SEI formation,[35, 36] the appearance of these two high-voltage peaks implies that  
20 the electrochemical reaction of silicon oxide with lithium is also involved during the first  
21 discharge process.[25] Besides these two high-voltage peaks, a sharp peak at ~0.05 V (low-  
22 voltage peak) is found in the initial discharge process at a current density of 20 mA/g (**Fig.**  
23 **5b**), and a broad peak at ~0.45 V could also be observed in the subsequent charge process.

1 This observation implies the occurrence of the lithiation of the Si phase during the  
2 discharge process and conversion of crystallized Li-Si alloy to an amorphous Si phase[34]  
3 during the subsequent charge process. Further reducing the current density to 10 mA/g  
4 leads to the significantly increased intensities of these two additional peaks during the  
5 initial cycle. In addition, it is worth noting that, regardless of the current density applied,  
6 no broad and/or sharp peaks are observed above 0.6 V during the subsequent charge  
7 process, indicating that the reaction of lithium with oxides is irreversible. The analysis of  
8 the differential capacity curves and voltage profiles suggests that the current density plays  
9 a crucial role in lithiating the Si phase in the Si@SiO<sub>x</sub> sample, and that there is a threshold  
10 value for the current density, ~10 mA/g here, below which the lithiation of the Si phase  
11 can take place in Si powders with a thick surficial oxide layer.

12 The low current density applied in the initial cycle has an “activating effect” and  
13 enables the high utilization of the Si phase in the Si@SiO<sub>x</sub> anode at high current densities  
14 during the following cycles. **Figure 6** exhibits voltage profiles of Si@SiO<sub>x</sub> anodes that  
15 were subjected to the same low current density of 10 mA/g during the initial cycles, but to  
16 higher current densities for the following cycles. Regardless of the current density used,  
17 the plateau-like feature observed on the initial cycle was replaced by a sloping potential in  
18 the 2<sup>nd</sup> and 3<sup>rd</sup> cycles for all cells, and the voltage curves of the 2<sup>nd</sup> and 3<sup>rd</sup> cycles for a  
19 given cell almost overlap, indicating excellent capacity retention. More importantly, an  
20 unprecedentedly high reversible capacity could be delivered by all cells in the 2<sup>nd</sup> and 3<sup>rd</sup>  
21 cycles even at high current densities. At a current density of 10 mA/g, the charge capacity  
22 of the 2<sup>nd</sup> and 3<sup>rd</sup> cycles is ~990 mAh/g, and it decreases slightly when the current density  
23 is increased, but still has a high value of ~ 729 mAh/g even at 100 mA/g (**Fig. 7a**). This

1 observation suggests that a low current density is only necessary in the initial cycle to  
2 enable the Si@SiO<sub>x</sub> anodes' high reversible capacities. Therefore, a low current density  
3 applied to cells in the initial cycle serves to “activate” the Si@SiO<sub>x</sub> and enable the repeated  
4 lithiation/delithiation of Si during the following cycles. In addition, the CE increases  
5 gradually from ~58% in the 1<sup>st</sup> cycle to ~85 % in the 2<sup>nd</sup> cycle, and reaches ~91% in the 3<sup>rd</sup>  
6 cycle (**Fig. 7b**) at a current density of 10 mA/g. With increasing current density, the CEs  
7 for each cycle remain almost constant. This observation implies the independence of the  
8 side reactions from the current density applied in the 2<sup>nd</sup> and 3<sup>rd</sup> cycles, and further verifies  
9 the “activating” effect of the low current density applied to the Si@SiO<sub>x</sub> anode in the initial  
10 cycle. This is the **first** report of the “activating” effect of current density on a Si anode with  
11 a thick surficial oxide layer.

12           A thick oxide layer is formed at the surface of Si powders after thermal treatment  
13 (**Figs. 1 to 3**). That is to say, the lithiation of the Si phase in Si@SiO<sub>x</sub> will start after the  
14 complete lithiation of oxides, owing to the relatively higher potentials for the formation of  
15 lithium silicate and/or lithium oxide compared with the formation of Li-Si alloys.[25] The  
16 reaction mechanism of lithium with silicon oxide is still under debate, and different  
17 reaction products are observed in lithiated silicon oxides.[1, 2] However, the thickness of  
18 the surficial oxide layer on Si@SiO<sub>x</sub> obtained after 800°C treatment is calculated to be  
19 ~22.5 nm, assuming that the lithiation product is Li<sub>4</sub>SiO<sub>4</sub> and assuming reaction  
20 mechanism 2 (**Table 3**). This value agrees well with those obtained from weight gain and  
21 TEM observations, given the underestimated capacity loss from the formation of SEI film  
22 used here for nanosized particles. These findings imply that Li<sub>4</sub>SiO<sub>4</sub> is the major lithiation  
23 product of Si@SiO<sub>x</sub> with the thick surficial oxide layer seen here. Compared with silicon

1 oxide,  $\text{Li}_4\text{SiO}_4$  has much higher electronic conductivity,[37] which could enhance the  
2 conductivity of  $\text{Si@SiO}_x$ . This hypothesis is corroborated by the FTIR analysis on the  
3 thermally treated powders, pristine and cycled electrodes, shown in **Figure 8**. The FTIR  
4 spectra of both thermally treated Si powders and the pristine electrode display two broad  
5  $\text{SiO}_2$  bands[21], one from 1000 to 1250  $\text{cm}^{-1}$  and the other from 765 to 865  $\text{cm}^{-1}$ . Both  
6 bands largely disappear from the FTIR spectrum of the cycled electrode, which is  
7 consistent with observations on the battery performance that most  $\text{SiO}_2$  was  
8 electrochemically reduced during the initial formation cycle with the low current density  
9 of 10 mA/g. More important, the FTIR spectrum of the cycled electrode shows a new mode  
10 at 833  $\text{cm}^{-1}$  with broad overlapping bands between 900 and 1200  $\text{cm}^{-1}$ , characteristics of  
11  $[\text{SiO}_4]^{2-}$  tetrahedral arrangements[38]. This suggests that  $\text{Li}_4\text{SiO}_4$  is the most likely product  
12 of lithiated oxide after one formation cycle, but we could rule out the formation of other  
13 silicates, such as  $\text{Li}_2\text{SiO}_3$ , and  $\text{Li}_2\text{O}$ . In addition, the carboxylate stretching mode at 1700  
14  $\text{cm}^{-1}$  from PAA binder[39] in the spectrum of the pristine electrode disappears in the  
15 spectrum of cycled electrode due to substitution of acidic protons from COOH groups in  
16 PAA by lithium ions after the formation cycle. The new mode at 1300  $\text{cm}^{-1}$  and the  
17 relatively increased intensity of the broad bands at 1400, 1559 and 1640  $\text{cm}^{-1}$  displayed in  
18 the spectrum of cycled electrode are the results of the formation of lithium carbonate[40],  
19 which is commonly found in SEI[41].

20 The formation of  $\text{Li}_4\text{SiO}_4$  with high conductivity could be further verified by EIS  
21 measurements shown in **Figure 9**. After discharge to the same capacity of ~100 mAh/g  
22 (**Fig. 4b**), the charge-transfer resistance ( $R_{ct}$ ), i.e., the intercept of the semicircle with the x  
23 axis in the middle frequency, for the cell at the low current density of 10 mA/g, is much

1 lower ( $\sim 510 \Omega$ ) than that at the high current density of 20 mA/g ( $\sim 940 \Omega$ ) (**Fig. 9a**). The  
2 lithiation of silica is a kinetic process. The lower the current density applied, the more silica  
3 lithiated.[31] Thus, the cell with low current density applied exhibits significantly reduced  
4 charge-transfer resistance because of the formation of a large amount of highly conductive  
5  $\text{Li}_4\text{SiO}_4$  in the surficial layer of the  $\text{Si}@\text{SiO}_x$ . Meanwhile, there exists a value of current  
6 density below which all surficial silica could be lithiated, making wrapped Si accessible to  
7 lithium at a given cutoff voltage in the discharge process. This hypothesis is confirmed by  
8 our experimental observation on the high capacity of  $\text{Si}@\text{SiO}_x$  anodes when the current  
9 density applied in the initial cycle was below a threshold value of 10 mA/g. It is worth  
10 noting that we cannot exclude the existence of other lithiation products, owing to the  
11 insufficient experimental data. In particular, the formation of  $\text{Li}_2\text{O}$ , which has superior Li-  
12 ion conductivity relative to silicon oxide,[42] in the surficial layer could also significantly  
13 reduce the charge-transfer resistance of the  $\text{Si}@\text{SiO}_x$  anode.

14 The reaction between lithium and silica to form  $\text{Li}_4\text{SiO}_4$  is irreversible, and the  
15 retention of  $\text{Li}_4\text{SiO}_4$  in the surficial layer will benefit the electrochemical performance of  
16  $\text{Si}@\text{SiO}_x$  anodes. The EIS spectra collected on  $\text{Si}@\text{SiO}_x$  anodes in various lithiated states  
17 with the low current density of 10 mA/g show that, as expected, the value of  $R_{\text{ct}}$  decreases  
18 during the discharge process and reaches its minimum at the end of the discharge process  
19 (**Fig. 9b**). However, the charge-transfer resistance of the  $\text{Si}@\text{SiO}_x$  anode at the end of the  
20 subsequent charge process is almost the same as that at the end of the discharge process.  
21 This observation implies that the reaction of lithium with silica is irreversible, or at least a  
22 major portion of the lithiated silica is retained at the end of the charge process. Once the  
23 lithiation of silicon oxide is completed, only reversible reactions of Si with lithium will

1 occur in the Si@SiO<sub>x</sub> anode during the following cycles, and the overpotential of the cell  
2 will be almost independent of the current density.[31] The reaction between lithium and  
3 silica to form Li<sub>4</sub>SiO<sub>4</sub> and Li<sub>2</sub>O is irreversible, and the substitution of silicon oxide by  
4 Li<sub>4</sub>SiO<sub>4</sub> and Li<sub>2</sub>O, with relatively higher electronic and ionic conductivity, in the surficial  
5 layer makes the inner Si accessible to lithium. This hypothesis is confirmed by our  
6 experimental observation that Si@SiO<sub>x</sub> anodes which underwent the initial cycle at a low  
7 current density of 10 mA/g could deliver the high capacity of ~ 729 mAh/g during the  
8 following cycles, even at the high current density of 100 mA/g. That is to say, the low  
9 current density applied in the initial cycle has an “activating” effect to endow Si@SiO<sub>x</sub>  
10 anodes with high capacity. It is worth noting that, owing to the limited experimental data,  
11 we cannot exclude the possibility that weak points, such as pinholes, cracks and defects,  
12 might form at the surficial layer during the initial cycle. The formation of these weak points  
13 is also irreversible, facilitating the lithiation of the oxide-coated Si anode,[27] and could  
14 also contribute to the “activating” effect observed here. In addition, the current density for  
15 “activation” depends on the thickness of the surficial oxide layer, and a relatively high  
16 current density might be sufficient to utilize the Si core with a thin oxide shell for the high  
17 capacity application, which has been reported by other researchers[21, 27].

#### 18 **4. Conclusions**

19 The effect of the current density on the electrochemical performance of Si anodes  
20 with thick surficial oxide layers was investigated here. Studies on the initial cycle show  
21 that there exists a threshold value of the current density applied to the cell, below which  
22 the utilization of the Si phase in Si@SiO<sub>x</sub> could be realized to endow cells with high  
23 capacity. The low current density also has an “activating” effect, such that the low current

1 density is necessary to lithiate silica in the initial cycle but is unnecessary to endow cells  
2 with high capacity during the following cycles. The analysis of EIS measurements indicates  
3 that the observations of a threshold value and an “activating” effect of the current density  
4 applied in the initial cycle are associated with the irreversible formation of lithium silicates  
5 with high conductivity.

## 6 **Acknowledgments**

7 We gratefully acknowledge support from the U.S. Department of Energy’s (DOE) Office  
8 of Energy Efficiency & Renewable Energy Vehicle Technologies Office. SEM and TEM  
9 studies were performed at the Center for Nanoscale Materials at Argonne National  
10 Laboratory, an Office of Science User Facility operated for the U.S. Department of Energy  
11 (DOE) Office of Science by Argonne National Laboratory. Argonne National Laboratory  
12 is operated for the DOE Office of Science by UChicago Argonne, LLC, under contract  
13 number DE-AC02-06CH11357. Part of this work was supported by funds from the Support  
14 for Faculty Scholars Award, the Faculty Research and Creative Activity Award, and the  
15 New Faculty Start Up Fund at Western Michigan University.

- 2 [1] Z. Liu, Q. Yu, Y. Zhao, R. He, M. Xu, S. Feng, S. Li, L. Zhou, L. Mai, Silicon oxides: a promising  
3 family of anode materials for lithium-ion batteries, *Chemical Society Reviews*, 48 (2019) 285-  
4 309.
- 5 [2] N. Yan, F. Wang, H. Zhong, Y. Li, Y. Wang, L. Hu, Q.W. Chen, Hollow Porous SiO<sub>2</sub> Nanocubes  
6 Towards High-performance Anodes for Lithium-ion Batteries, *Sci Rep-Uk*, 3 (2013).
- 7 [3] A.A. Arie, W. Chang, J.K. Lee, Electrochemical characteristics of semi conductive silicon anode  
8 for lithium polymer batteries, *Journal of Electroceramics*, 24 (2010) 308-312.
- 9 [4] N. Liu, Z. Lu, J. Zhao, M.T. McDowell, H.-W. Lee, W. Zhao, Y. Cui, A pomegranate-inspired  
10 nanoscale design for large-volume-change lithium battery anodes, *Nature nanotechnology*, 9  
11 (2014) 187.
- 12 [5] J.-H. Cho, S.T. Picraux, Silicon nanowire degradation and stabilization during lithium cycling  
13 by SEI layer formation, *Nano letters*, 14 (2014) 3088-3095.
- 14 [6] J.-L. Zang, Y.-P. Zhao, Silicon nanowire reinforced by single-walled carbon nanotube and its  
15 applications to anti-pulverization electrode in lithium ion battery, *Composites Part B:  
16 Engineering*, 43 (2012) 76-82.
- 17 [7] G. Zhou, H. Li, H. Sun, D. Yu, Y. Wang, X. Huang, L. Chen, Z. Zhang, Controlled Li doping of Si  
18 nanowires by electrochemical insertion method, *Applied physics letters*, 75 (1999) 2447-2449.
- 19 [8] G. Wang, J. Ahn, J. Yao, S. Bewlay, H. Liu, Nanostructured Si-C composite anodes for lithium-  
20 ion batteries, *Electrochemistry communications*, 6 (2004) 689-692.
- 21 [9] S. Bourderau, T. Brousse, D. Schleich, Amorphous silicon as a possible anode material for Li-  
22 ion batteries, *Journal of power sources*, 81 (1999) 233-236.
- 23 [10] L.-F. Cui, L. Hu, J.W. Choi, Y. Cui, Light-weight free-standing carbon nanotube-silicon films  
24 for anodes of lithium ion batteries, *ACS nano*, 4 (2010) 3671-3678.
- 25 [11] M.K. Datta, P.N. Kumta, Silicon and carbon based composite anodes for lithium ion  
26 batteries, *Journal of Power Sources*, 158 (2006) 557-563.
- 27 [12] S.-L. Chou, J.-Z. Wang, M. Choucair, H.-K. Liu, J.A. Stride, S.-X. Dou, Enhanced reversible  
28 lithium storage in a nanosize silicon/graphene composite, *Electrochemistry Communications*, 12  
29 (2010) 303-306.
- 30 [13] Y. NuLi, B. Wang, J. Yang, X. Yuan, Z. Ma, Cu<sub>5</sub>Si-Si/C composites for lithium-ion battery  
31 anodes, *Journal of power sources*, 153 (2006) 371-374.
- 32 [14] S.H. Ng, J. Wang, D. Wexler, S.Y. Chew, H.K. Liu, Amorphous carbon-coated silicon  
33 nanocomposites: a low-temperature synthesis via spray pyrolysis and their application as high-  
34 capacity anodes for lithium-ion batteries, *The Journal of Physical Chemistry C*, 111 (2007) 11131-  
35 11138.
- 36 [15] W. Wang, P.N. Kumta, Nanostructured hybrid silicon/carbon nanotube heterostructures:  
37 reversible high-capacity lithium-ion anodes, *ACS nano*, 4 (2010) 2233-2241.
- 38 [16] M.T. McDowell, S.W. Lee, I. Ryu, H. Wu, W.D. Nix, J.W. Choi, Y. Cui, Novel Size and Surface  
39 Oxide Effects in Silicon Nanowires as Lithium Battery Anodes, *Nano Letters*, 11 (2011) 4018-  
40 4025.
- 41 [17] H. Wu, G. Chan, J.W. Choi, I. Ryu, Y. Yao, M.T. McDowell, S.W. Lee, A. Jackson, Y. Yang, L.B.  
42 Hu, Y. Cui, Stable cycling of double-walled silicon nanotube battery anodes through solid-  
43 electrolyte interphase control, *Nature Nanotechnology*, 7 (2012) 309-314.
- 44 [18] Y. Chen, L.F. Liu, J. Xiong, T.Z. Yang, Y. Qin, C.L. Yan, Porous Si Nanowires from Cheap  
45 Metallurgical Silicon Stabilized by a Surface Oxide Layer for Lithium Ion Batteries, *Adv Funct  
46 Mater*, 25 (2015) 6701-6709.

1 [19] G.B. Zhu, Y. Wang, S.M. Yang, Q.T. Qu, H.H. Zheng, Correlation between the physical  
2 parameters and the electrochemical performance of a silicon anode in lithium-ion batteries, *J*  
3 *Materiomics*, 5 (2019) 164-175.

4 [20] S. Sim, P. Oh, S. Park, J. Cho, Critical thickness of SiO<sub>2</sub> coating layer on core@ shell bulk@  
5 nanowire Si anode materials for Li-ion batteries, *Advanced Materials*, 25 (2013) 4498-4503.

6 [21] L.H. Zhang, Y.Z. Liu, B. Key, S.E. Trask, Z.Z. Yang, W.Q. Lu, Silicon Nanoparticles: Stability in  
7 Aqueous Slurries and the Optimization of the Oxide Layer Thickness for Optimal Electrochemical  
8 Performance, *Acs Appl Mater Inter*, 9 (2017) 32727-32736.

9 [22] T. Kim, S. Park, S.M. Oh, Solid-state NMR and electrochemical dilatometry study on Li+  
10 uptake/extraction mechanism in SiO electrode, *J Electrochem Soc*, 154 (2007) A1112-A1117.

11 [23] H. Takezawa, K. Iwamoto, S. Ito, H. Yoshizawa, Electrochemical behaviors of  
12 nonstoichiometric silicon suboxides (SiO<sub>x</sub>) film prepared by reactive evaporation for lithium  
13 rechargeable batteries, *Journal of Power Sources*, 244 (2013) 149-157.

14 [24] B.K. Guo, J. Shu, Z.X. Wang, H. Yang, L.H. Shi, Y.N. Liu, L.Q. Chen, Electrochemical reduction  
15 of nano-SiO<sub>2</sub> in hard carbon as anode material for lithium ion batteries, *Electrochemistry*  
16 *Communications*, 10 (2008) 1876-1878.

17 [25] Q. Sun, B. Zhang, Z.W. Fu, Lithium electrochemistry of SiO<sub>2</sub> thin film electrode for lithium-  
18 ion batteries, *Appl Surf Sci*, 254 (2008) 3774-3779.

19 [26] C.M. Ban, B.B. Kappes, Q. Xu, C. Engtrakul, C.V. Ciobanu, A.C. Dillon, Y.F. Zhao, Lithiation of  
20 silica through partial reduction, *Applied Physics Letters*, 100 (2012).

21 [27] M. Schnabel, S.P. Harvey, E. Arca, C. Stetson, G. Teeter, C.M. Ban, P. Stradins, Surface SiO<sub>2</sub>  
22 Thickness Controls Uniform-to-Localized Transition in Lithiation of Silicon Anodes for Lithium-Ion  
23 Batteries, *Acs Appl Mater Inter*, 12 (2020) 27017-27028.

24 [28] B. Philippe, R. Dedryvere, M. Gorgoi, H. Rensmo, D. Gonbeau, K. Edstrom, Improved  
25 Performances of Nanosilicon Electrodes Using the Salt LiFSI: A Photoelectron Spectroscopy  
26 Study, *J Am Chem Soc*, 135 (2013) 9829-9842.

27 [29] E. Sivonxay, M. Aykol, K.A. Persson, The lithiation process and Li diffusion in amorphous  
28 SiO<sub>2</sub> and Si from first-principles, *Electrochim Acta*, 331 (2020).

29 [30] S.D. Han, K.N. Wood, C. Stetson, A.G. Norman, M.T. Brumbach, J. Coyle, Y. Xu, S.P. Harvey,  
30 G. Teeter, A. Zakutayev, A.K. Burrell, Intrinsic Properties of Individual Inorganic Silicon-  
31 Electrolyte Interphase Constituents, *Acs Appl Mater Inter*, 11 (2019) 46993-47002.

32 [31] J.K. Lee, W.Y. Yoon, B.K. Kim, Kinetics of Reaction Products of Silicon Monoxide with  
33 Controlled Amount of Li-Ion Insertion at Various Current Densities for Li-Ion Batteries, *J*  
34 *Electrochem Soc*, 161 (2014) A927-A933.

35 [32] H. Hamdan, M.N.M. Muhid, S. Endud, E. Listiorini, Z. Ramli, <sup>29</sup>Si MAS NMR, XRD and FESEM  
36 studies of rice husk silica for the synthesis of zeolites, *Journal of Non-Crystalline Solids*, 211  
37 (1997) 126-131.

38 [33] X. Liu, J.Q. Huang, Q. Zhang, L. Mai, Nanostructured Metal Oxides and Sulfides for Lithium-  
39 Sulfur Batteries, *Adv Mater*, 29 (2017).

40 [34] T.D. Hatchard, J.R. Dahn, In situ XRD and electrochemical study of the reaction of lithium  
41 with amorphous silicon, *J Electrochem Soc*, 151 (2004) A838-A842.

42 [35] C.K. Chan, R. Ruffo, S.S. Hong, Y. Cui, Surface chemistry and morphology of the solid  
43 electrolyte interphase on silicon nanowire lithium-ion battery anodes, *Journal of Power Sources*,  
44 189 (2009) 1132-1140.

45 [36] A.L. Michan, M. Leskes, C.P. Grey, Voltage Dependent Solid Electrolyte Interphase  
46 Formation in Silicon Electrodes: Monitoring the Formation of Organic Decomposition Products,  
47 *Chem Mater*, 28 (2016) 385-398.

- 1 [37] Y. Zhang, Y. Li, Z. Wang, K. Zhao, Lithiation of SiO<sub>2</sub> in Li-ion batteries: in situ transmission  
2 electron microscopy experiments and theoretical studies, *Nano letters*, 14 (2014) 7161-7170.
- 3 [38] D. Cruz, S. Bulbulian, Synthesis of Li<sub>4</sub>SiO<sub>4</sub> by a modified combustion method, *J Am Ceram*  
4 *Soc*, 88 (2005) 1720-1724.
- 5 [39] W. Kam, C.W. Liew, J.Y. Lim, S. Ramesh, Electrical, structural, and thermal studies of  
6 antimony trioxide-doped poly(acrylic acid)-based composite polymer electrolytes, *Ionics*, 20  
7 (2014) 665-674.
- 8 [40] R.T. Pekarek, A. Affolter, L.L. Baranowski, J. Coyle, T.Z. Hou, E. Sivonxay, B.A. Smith, R.D.  
9 McAuliffe, K.A. Persson, B. Key, C. Apblett, G.M. Veith, N.R. Neale, Intrinsic chemical reactivity of  
10 solid-electrolyte interphase components in silicon-lithium alloy anode batteries probed by FTIR  
11 spectroscopy, *J Mater Chem A*, 8 (2020) 7897-7906.
- 12 [41] R.E. Ruther, K.A. Hays, S.J. An, J.L. Li, D.L. Wood, J. Nanda, Chemical Evolution in Silicon-  
13 Graphite Composite Anodes Investigated by Vibrational Spectroscopy, *Acs Appl Mater Inter*, 10  
14 (2018) 18641-18649.
- 15 [42] S.C. Jung, H.J. Kim, J.H. Kim, Y.K. Han, Atomic-Level Understanding toward a High-Capacity  
16 and High Power Silicon Oxide (SiO) Material, *Journal of Physical Chemistry C*, 120 (2016) 886-  
17 892.
- 18
- 19

1  
2  
3  
4  
5  
6  
7  
8  
9  
10  
11  
12  
13  
14  
15  
16  
17

**Table 1.** Thickness of surficial oxide layer on Si@SiO<sub>x</sub> after thermal treatment at various temperatures

| Temperature (°C) | Weight gain (%) | Weight ratio of SiO <sub>2</sub> (%) | Calculated thickness of SiO <sub>2</sub> layer (nm) |
|------------------|-----------------|--------------------------------------|---|
| <b>600</b>       | 13.3            | 33.6                                 | 5.6   |
| <b>700</b>       | 32.5            | 56.8                                 | 11.2  |
| <b>800</b>       | 59.6            | 78.9                                 | 19.6  |
| <b>900</b>       | 60.5            | 79.6                                 | 20.0  |
| <b>1000</b>      | 61.8            | 80.2                                 | 20.3  |

The following assumptions were used to calculate the weight ratio and thickness of the surficial oxide layer:

1. Initial particle has a spherical shape.
2. Initial particle has a Si core with a radius of 38 nm, and a 2-nm-thick SiO<sub>2</sub> shell.

1  
2  
3  
4  
5  
6  
7  
8  
9  
10  
11  
12  
13  
14  
15  
16  
17  
18  
19  
20  
21

**Table 2.** Summary of electrochemical performance of Si@SiO<sub>x</sub> anode at various current densities in the initial cycles

| <b>Current density (mA/g)</b> | <b>Discharge capacity (mAh/g)</b> | <b>Charge capacity (mAh/g)</b> | <b>Capacity loss (mAh/g)</b> | <b>Coulombic efficiency (%)</b> |
|-------------------------------|-----------------------------------|--------------------------------|------------------------------|---------------------------------|
| <b>10</b>                     | 1832                              | 1063                           | 769                          | 58                              |
| <b>20</b>                     | 97                                | 38                             | 59                           | 39                              |
| <b>50</b>                     | 71                                | 27                             | 44                           | 38                              |
| <b>100</b>                    | 68                                | 26                             | 42                           | 38                              |

1 **Table 3.** Thickness of surficial oxide layer of 800°C-treated Si@SiO<sub>x</sub> anode,  
 2 calculated from electrochemical performance

| Mechanism      | Reaction equations  | Irreversible lithiation product  | Weight ratio of SiO <sub>2</sub> (%) | Calculated thickness of SiO <sub>2</sub> layer (nm) |
|----------------|---|----------------------------------|--------------------------------------|---|
| 1 <sup>1</sup> | $5SiO_2 + 4Li^+ + 4e \leftrightarrow 2Li_2Si_2O_5 + Si$<br>$5Si + 22Li^+ + 22e \leftrightarrow Li_{22}Si_5$ | N/A                              | N/A                                  | N/A   |
| 2 <sup>2</sup> | $2SiO_2 + 4Li^+ + 4e \rightarrow 2Li_4SiO_4 + Si$<br>$5Si + 22Li^+ + 22e \leftrightarrow Li_{22}Si_5$       | Li <sub>4</sub> SiO <sub>4</sub> | 83.9                                 | 22.5  |
| 3 <sup>2</sup> | $SiO_2 + 4Li^+ + 4e \leftrightarrow 2Li_2O + Si$<br>$5Si + 22Li^+ + 22e \leftrightarrow Li_{22}Si_5$        | Li <sub>2</sub> O                | 42.0                                 | 7.4   |

3 The following assumptions were used to calculate the thickness of the surficial oxide  
 4 layer from electrochemical data:

- 5 1. Silicon in the core of Si@SiO<sub>x</sub> was not involved in the lithiation process when the  
 6 current density was above 20 mA/g.
- 7 2. Capacity loss is only associated with the formation of SEI and irreversible lithiation  
 8 product.
- 9 3. The reaction between Si and lithium is reversible.

10

1  
2  
3  
4  
5  
6  
7  
8  
9  
10  
11  
12  
13  
14  
15

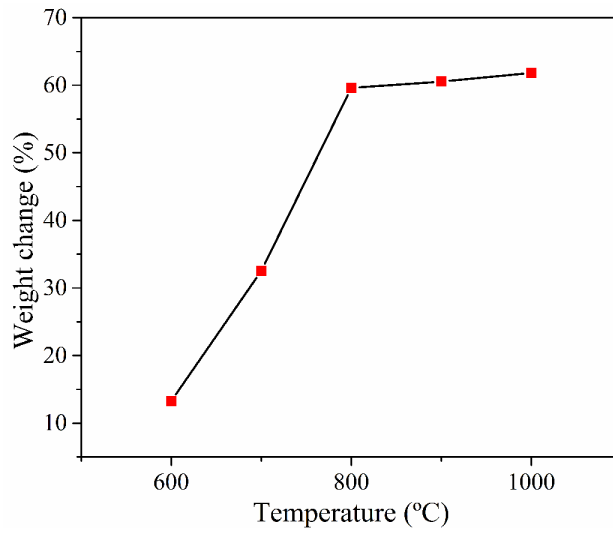


**Figure 1.** The weight change of silicon powders as a function of the temperature of the thermal treatment.

1  
2  
3  
4  
5  
6  
7  
8  
9  
10  
11  
12  
13  
14  
15  
16  
17  
18  
19  
20

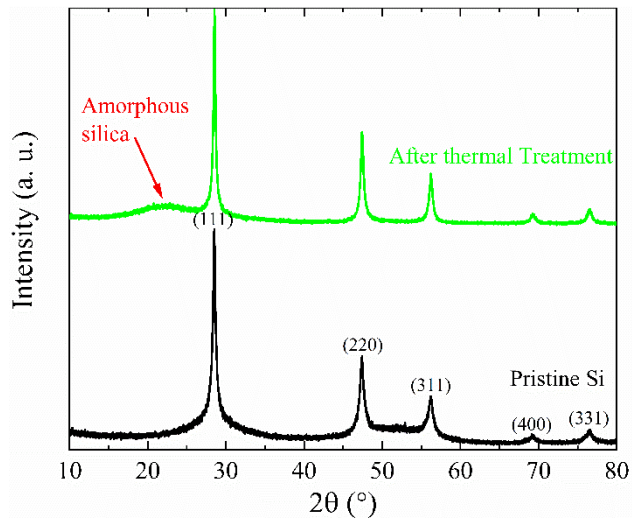


**Figure 2.** X-ray diffraction patterns of pristine and thermally oxidized silicon powders.

The thermal treatment was conducted at 800°C for 15 hours.

1

2

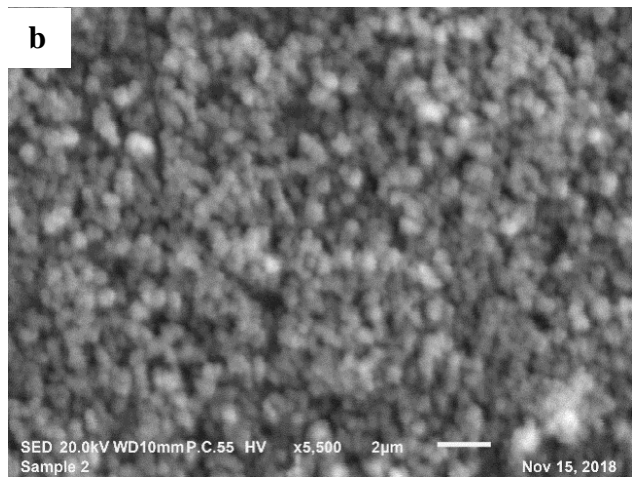
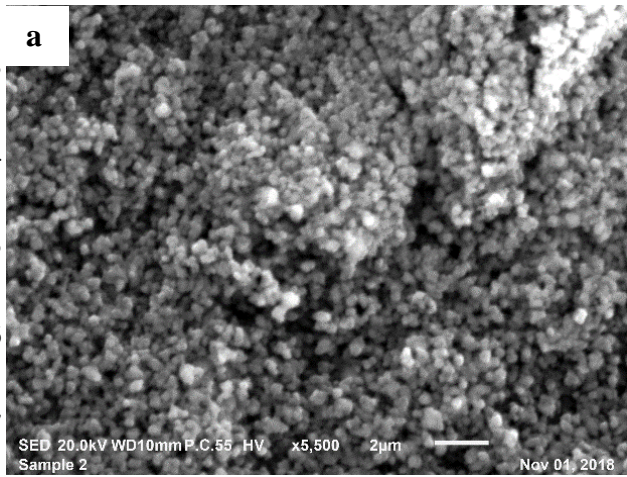
3

4

5

6

7



8

9

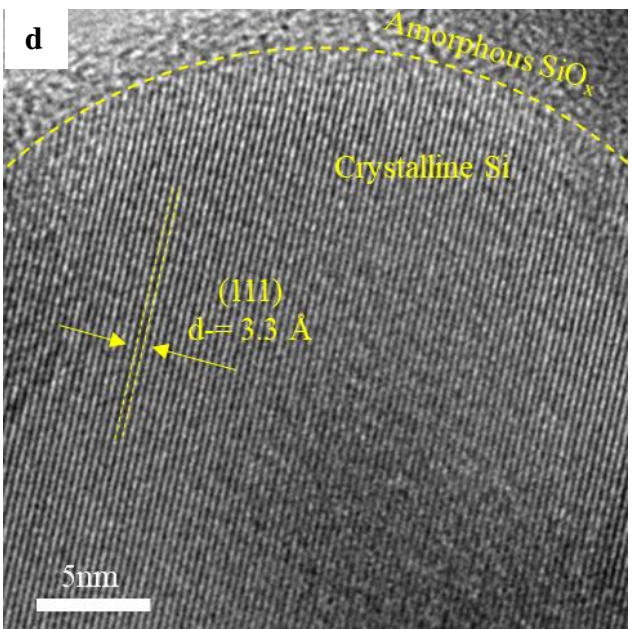
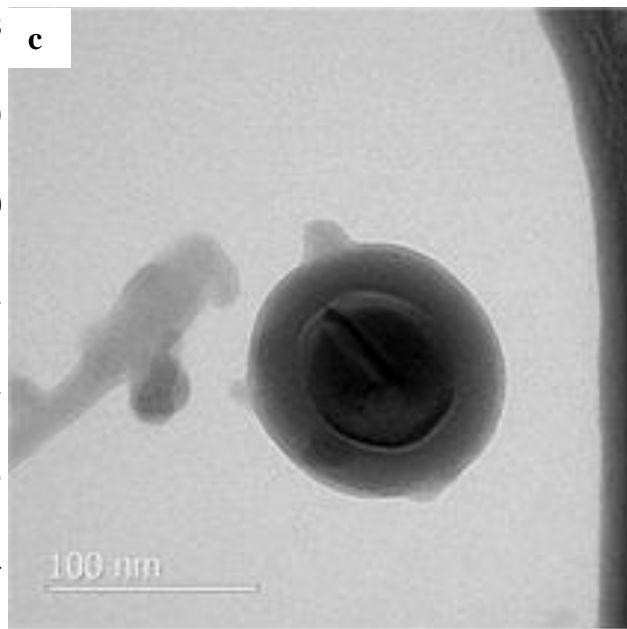
10

11

12

13

14



15

16

17

18

19

20

**Figure 3.** SEM images of pristine (a) and thermally oxidized (b) Si powders. Low (c) and high (d) magnification TEM images of thermally oxidized Si powder. The thermal treatment was conducted at 800°C for 15 hours. The dashed line in panel d shows the boundary between the crystalline core with a single orientation of lattice fringes and amorphous oxide shell.

1

2

3

4

5

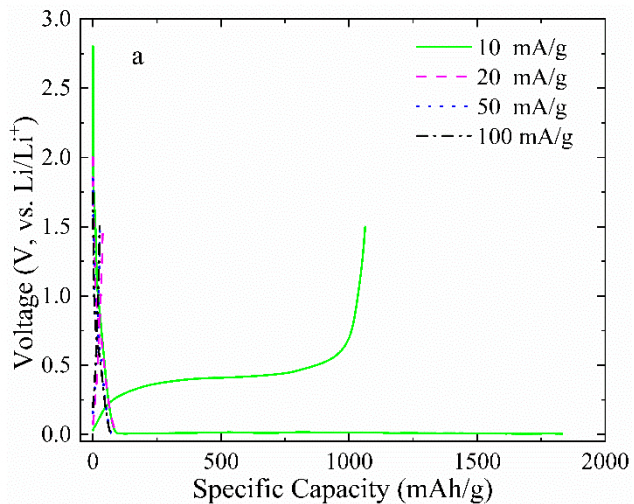
6

7

8

9

10



11

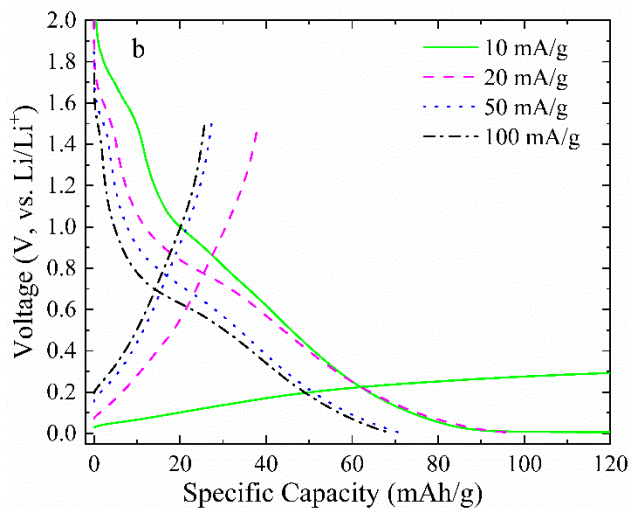
12

13

14

15

16



17

**Figure 4.** Full (a) and enlarged (b) voltage profiles of Si@SiO<sub>x</sub> anodes at various current densities during the initial cycles.

19

1  
2  
3  
4  
5  
6  
7  
8  
9  
10  
11  
12  
13  
14  
15  
16  
17  
18  
19  
20

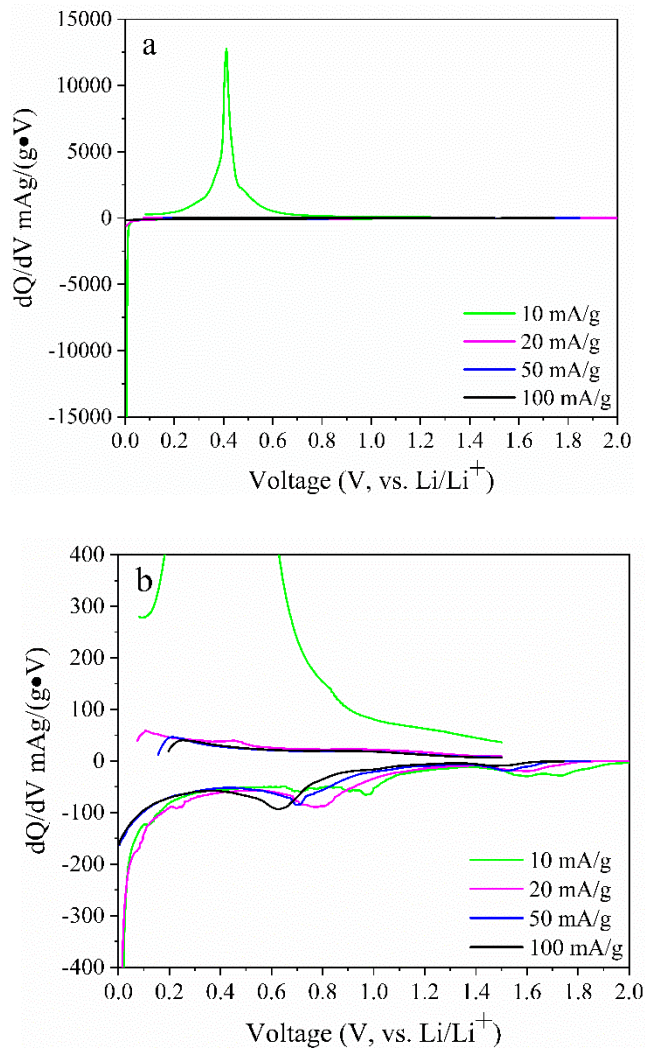


**Figure 5.** Full (a) and enlarged (b) differential capacity curves of cells with Si@SiO<sub>x</sub> anodes at various current densities during the initial cycle.

1  
2  
3  
4  
5  
6  
7  
8  
9  
10  
11  
12  
13  
14  
15  
16  
17  
18  
19  
20

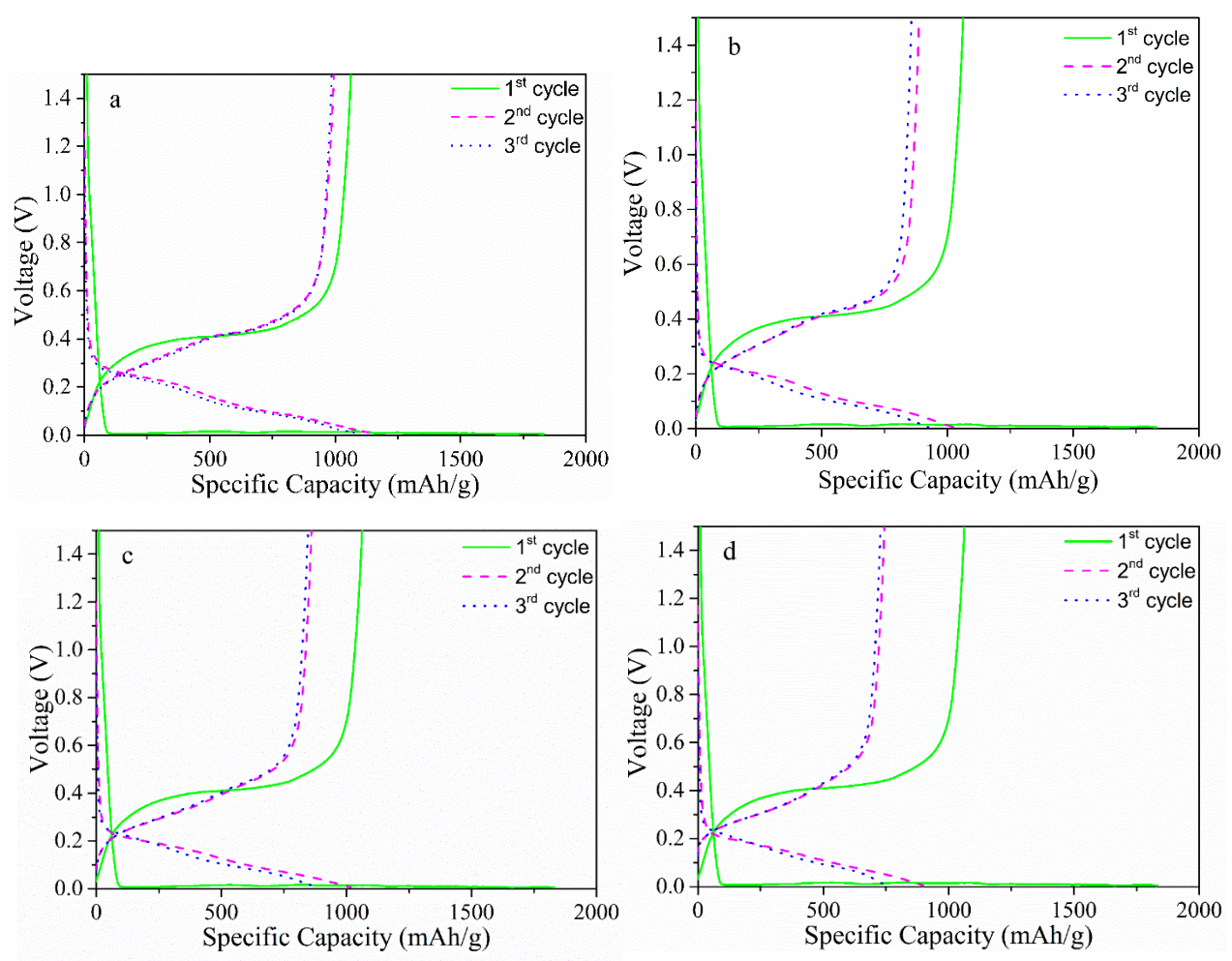


**Figure 6.** Voltage profiles of cells with Si@SiO<sub>x</sub> anodes at a current density of 10 mA/g (a), 20 mA/g (b), 50 mA/g (c), and 100 mA/g (d) during the 2<sup>nd</sup> and 3<sup>rd</sup> cycles. The same current density of 10 mA/g was applied to all cells in the initial cycles.

1

2

3

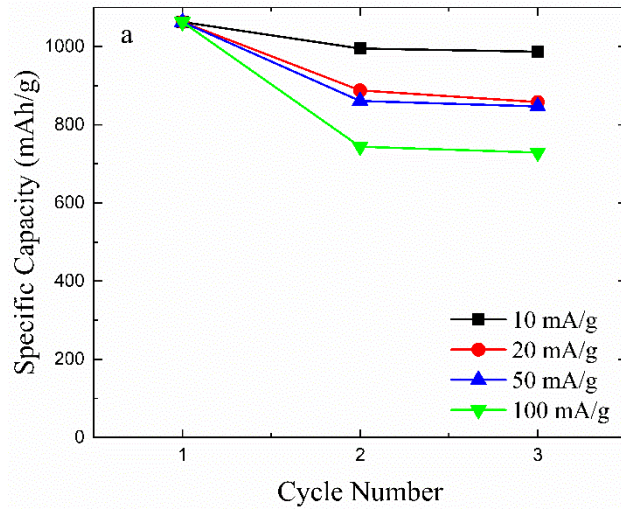
4

5

6

7

8



9

10

11

12

13

14

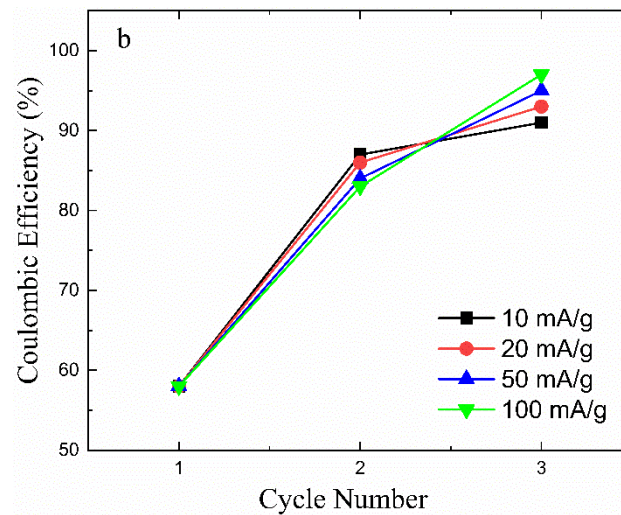


**Figure 7.** The dependence of specific capacity (a) and coulombic efficiency (b) on the current densities applied in the 2<sup>nd</sup> and 3<sup>rd</sup> cycles. The same current density of 10 mA/g was applied to all cells in the initial cycles.

18

19

20

1  
2  
3  
4  
5  
6  
7  
8  
9  
10  
11  
12  
13  
14  
15  
16  
17  
18  
19  
20

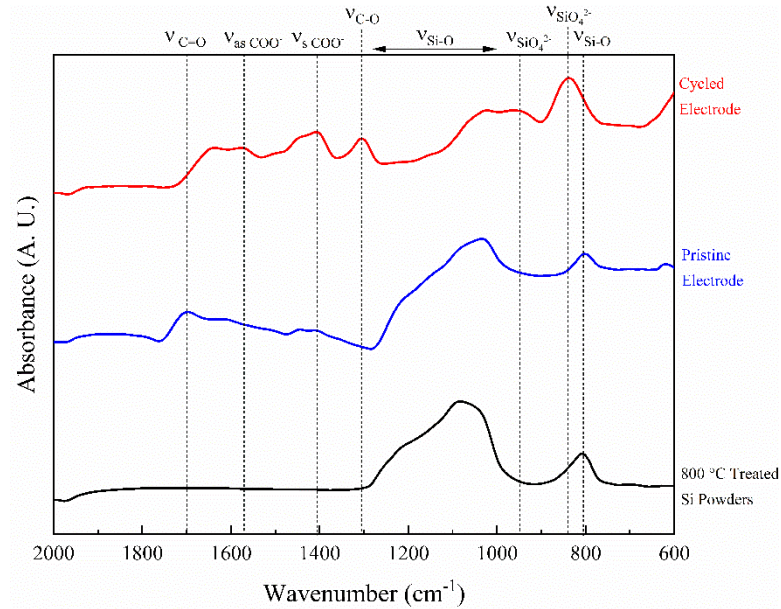


**Figure 8.** FTIR spectra of the thermally treated Si powders, the pristine and cycled electrodes containing thermally treated Si. The thermal treatment on Si powders was conducted at 800°C for 15 hours. The cycled electrodes were harvested from cells underwent discharge with the current density of 10 mA/g and then charged to 1.5V.

1

2

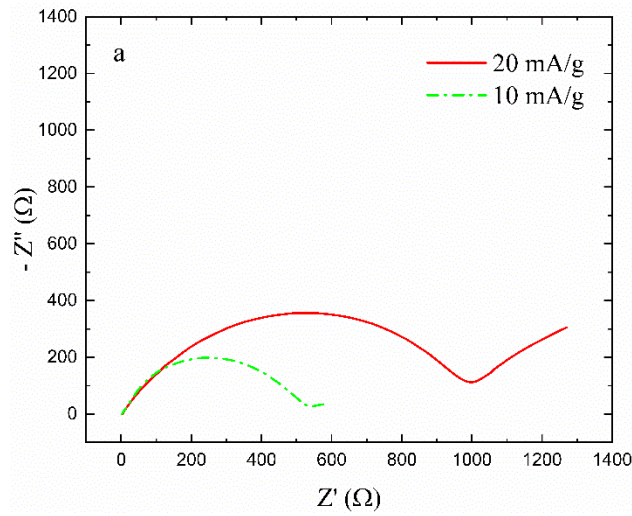
3

4

5

6

7



8

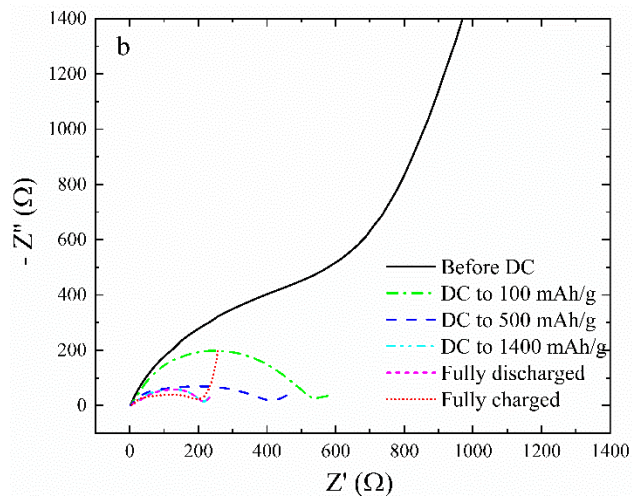
9

10

11

12

13



14

**Figure 9.** EIS of Si@SiO<sub>x</sub> anodes discharged to the same capacity of 100 mAh/g

15

with different current densities (a), and to various depth of discharge states (b) with the

16

same current density of 10 mA/g.

17

18

19